Effect of the Boson Peak and the Ionic Resonance in the Dielectric Properties of Silicate Materials at mm-Wave and THz Frequencies

Rodriguez-Cano, Rocio; Lanagan, Michael

Published in:
Materials Research Bulletin

Publication date:
2024

Document Version
Accepted author manuscript, peer reviewed version

Effect of the Boson Peak and the Ionic Resonance in the Dielectric Properties of Silicate Materials at mm-Wave and THz Frequencies

Rocio Rodriguez-Cano[a,b], Michael T. Lanagan[b]

[a]*Electronic Systems Department. APMS section. Aalborg University, 9220 Aalborg East, Denmark*
[b]*Materials Research Institute. Penn State University, 16802 University Park, PA, USA*

Abstract

In this paper, a broadband measurement of the dielectric properties of silicates has been done to cover the seldom characterized mm-wave spectrum and the low THz spectrum. The dielectric properties, **i.e. loss and permittivity, show a frequency independent** response **up to** approximately 40 GHz and the loss monotonically increases to the THz frequency range. Two resonance peaks appear at THz frequencies: the first is the boson peak, and the second one corresponds to the ionic resonance of the network former, which in this case is silicon. Even though the materials belong to different groups in the silicate family **(crystalline and non-crystalline, with different levels of purity)**, they seem to have the same overall tendency **in the dielectric properties**. Argand plots are used for the first time at THz frequencies to provide physical insight into the boson peak and ionic resonance. The complex plane analysis reveals details on the polarization mechanisms underlying silicate network vibrations through direct visualization of their characteristic signatures, **and simplifies the process of modeling the dielectric response, leading to a better fit**.

Keywords:
Cole-Cole, dielectric, characterization, mm-wave, silicates, THz, 5G, 6G

1. Introduction

The inclusion of new frequency bands in the millimeter-wave (mm-wave) spectrum for 5G communications and the prospect of more frequency bands up to the low terahertz (THz) for 6G has prompted new efforts in assessing and analyzing the dielectric behavior of materials at those frequencies. However, the THz band, covering frequencies from around 0.1 to 10 THz, has historically been difficult to generate and detect using conventional electronic or optical techniques. The lack of data at these frequencies has caused the regime to be denominated as the "THz measurement gap" [1]. The development of femtosecond laser pulses, which enable the generation of THz radiation via time-domain spectroscopy (TDS), and techniques like Fourier transform infrared spectroscopy (FTIR) are helping bridge the THz gap. For instance, several glasses have been measured from 0.1 – 2 THz in [2] and from 0.5 – 15 THz in [3].

The dielectric relaxation in solids is a broadly studied topic in literature and yet it is not fully understood. Moreover, the lack of available dielectric measurement data in the THz gap hampers the definitive characterization of the spectral locations, where certain resonances occur, and the boundaries between regimes, where different analytical models apply. The region from low Hz to GHz is said to be characterized by the universal frequency dependence, which may involve superimposed dipolar processes. This region is dominated by many-body interactions and it is weakly thermally activated, unlike lower frequency regions [4]. The universal relaxation law can be written in terms of the complex susceptibility, χ, as

$$\chi'' = \begin{cases} \propto \omega^m & \text{for the rising part with } \omega \ll \omega_p \\ \cot(n\pi/2)\,\chi' \;\propto \omega^{n-1} & \text{for the falling part with } \omega \gg \omega_p, \end{cases} \tag{1}$$

with ω_p the loss peak frequency and the exponents m and n fall in the range (0,1). The complex permittivity can be calculated from the susceptibility as

$$\epsilon_r = 1 + \chi = (1 + \chi') + i \cdot \chi''. \quad (2)$$

However, many low-loss materials differ significantly from the universal relation. One of these cases corresponds to the flat-loss model in several decades of the permittivity spectrum, located between two relaxations. The flat, low-loss dielectric spectrum has conventionally been viewed as the limiting case of the universal power law model as the exponent n approaches 1, which leads to $\chi''(\omega)/\chi'(\omega) \rightarrow 0$. However, other proposed models not obeying the universal law also exhibit low, flat loss without following the relation in Equation (1). The physical significance of the cotangent relationship from Equation (1) is that it directly correlates the dielectric loss to the polarization, independent of frequency. This suggests a constant energy dissipation occurs per each reversal of the microscopic polarization [5, 6]. As possible explanation, the interaction with the surrounding medium is one of the proposed mechanisms for a constant energy loss per reversal of microscopic polarization, leading to flat, low-loss dielectric spectra [6]. However, other mechanisms can also give rise to such behavior. These include the reorientation of polar side groups on polymer chains [7], screened charge carrier hopping between defects [4], and slow ionic motions in materials exhibiting low-frequency dispersion [8].

As frequency increases into the mm-wave and THz ranges, the **movement of the charges** cannot keep up with the oscillating field. Shorter wavelength phonon vibrations and optical resonances occur instead. In [4], A.K Jonscher wrote about the expectancy of a loss peak in the optical frequency region, due to quantum transitions. Earlier low-frequency Raman spectra of **vitreous** SiO_2 has shown that there are actually two dominant peaks in the spectrum, a boson peak and a broad peak [9]. The broad band peak was studied by Galeener [10] and it was attributed to the bending motion of Si-O-Si bridges, which corresponds to the ionic resonance. The origin of the boson peak is still being discussed in solid-state physics, but it appears to be a common feature of the glassy state. In [9], they associate the boson peak to localized vibrations, which can be modelled by a harmonic oscillator, whose vibrational frequency is mainly determined by the reduced mass of the oscillator. According to [11], the boson peak does not only originate from structural disorder, since it is also present in the spectrum for a same-density crystalline phase, as a sharper feature. Moreover, the nature of this disorder influences the mode distribution affecting the boson peak and the heat capacity of the glass. The two peaks, i.e. boson peak and Si-O-Si bending vibration, can be seen in different compositions of sodium silicate glasses. The intensity of the boson peak increases with the sodium percentage, while the opposite behaviour is found in the ionic resonance [3].

This paper aims to clarify the applicability of the universal and flat-loss dielectric models to silicate materials in the gigahertz part of the spectrum. In the mm-wave and low-THz frequencies, the goal is to identify the possible resonances and if they have a common behavior in silicates. A broadband characterization of the dielectric properties from 5 GHz to 18 THz frequencies has been provided. We present extensive experimental dielectric spectra of various silicate families, obtained using techniques spanning microwaves to optics. By combining the precise resonant measurement techniques, free-space measurements, and THz-TDS and FTIR in the far-IR, we acquire permittivity and loss tangent values over an unprecedented frequency range. The analysis of the broadband silicate data enables assessment of whether the characteristic low-loss spectral shape follows the theoretical predictions of the universal response or exhibits the flat loss phenomenon in between relaxations. This comprehensive investigation of the dielectric properties from GHz to THz frequencies of silicates will provide unique insight into the appropriate analytic forms for predicting their dielectric function and advance understanding of their polarization and loss mechanisms.

2. Materials and Methods

Silicate materials can be categorized as either crystalline, such as quartz, or amorphous, such as fused silica and glass, based on their internal atomic structure and order. Crystalline materials have lower dielectric losses, as they have tightly bound atoms in fixed orientations. In this paper, we characterize mainly non-crystalline materials, since they have more loosely bound entities that are more polarizable with the application of an electric field [12]. The percentage of impurities added in amorphous materials causes the depolymerization of the silica network and, therefore, the higher loss. The characterized materials are listed in Table 1. The acronym FS corresponds to fused silica, and the FS designations represent different synthesis routes. The JGS2 is formed through a melt process, and the other FS designations are formed through a fumed process. The composition of some of the measured materials has been obtained by inductively coupled plasma (ICP) analysis and it is listed in [13]. Most of the commercial glasses have a high alkali percentage, followed by aluminum, boron and/or alkaline earth elements.

Table 1. Thickness of the characterized materials.

Material	Thickness (mm)	Material	Thickness (mm)
Quartz	0.5	Borofloat 33	0.5
FS-518	0.5	Gorilla Glass	0.5
FS-JGS2	1	AF45	0.31
FS-HFM002.B2	0.515	OA-10G	0.7
FS-7980	0.5	Window glass	2.3
BK7	0.5	D263	0.5

We have utilized a range of complementary techniques to obtain the broadband dielectric spectra of silicate materials from the gigahertz into the terahertz regions. In the GHz ranges, split-post resonators, split-cylinder cavities, and open Fabry-Perot resonators provide precise dielectric data. **The split cavity is the measurement method which provides the maximum error among these low frequency techniques,** $\pm 1\%$ **in the real part of the permittivity. Regarding the loss,** $\tan\delta < 1e^{-4}$ **[13].** As frequency increases above 100 GHz, characterization becomes more challenging. **Around that frequency, the material characterization kit (MCK) from SWISSto12 has an accuracy of** $\epsilon_r \pm 1\%$ **and** $\tan\delta \pm 5\%$**.** We have employed THz time-domain spectroscopy (THz-TDS) to cover 0.3 – 2.5 THz. **The percentage error for THz-TDS is around** 1% **[14].** Finally, extending measurements into the far-IR from 2 – 18 THz is enabled by Fourier transform infrared (FTIR) spectroscopy. **FTIR can only measure magnitude values of transmission or reflection. In order to obtain the phase information, the Kramers-Kronig analysis need to be employed. The error from the approximation to obtain the loss is typically** 1%**, and in general, will not exceed** 10% **[15]**. This multi-technique metrology provides almost seamless broadband characterization. A detailed analysis of the capabilities and limitations of these tools for quantitative dielectric measurement of silicates is given in our previous work [13, 16]. A key finding from the FTIR measurements is the revelation of two strong absorption resonances in the far-IR around 2.3 and 13 THz, which reveal the presence of lattice vibrational modes. By uniting together data across diverse methods spanning GHz to THz frequencies, we have assembled an unprecedented dielectric spectrum revealing the location of the boson peak and the ionic resonance in the THz gap, which are common for all the different groups silicates and will be discussed in the next section.

3. Results

The complete measurement results covering the mm-wave spectrum and THz gap have been plotted in Fig. 1. A **frequency independent dielectric** response can be seen in the GHz frequencies for both fused silicas and glasses, which demonstrates that silicate materials adhere closely to the flat-loss response model proposed by Jonscher [5] **up to** 40 GHz. Fused silicas have a dielectric constant of 4, while the glasses have higher values due to the inclusion of modifiers in the silica network [13]. The higher purity of the fused silicas **causes** them to have lower loss values in this frequency range. As it was mentioned in the introduction, two resonances appear in the dielectric constant at THz frequencies. These resonances have loss peaks counterparts in the loss tangent plot. The first resonance appears between 2 and 3 THz and corresponds to the boson peak, an anomalous excess in the vibrational density of states compared to the prediction from Debye theory for crystalline materials. In alkali silicates, i.e. the commercial glasses **listed in the second column of Table 1 together with BK7**, the boson peak is thought to be made up of two independent contributions. The first involves coupled motions (libration and distortion) of SiO_4 tetrahedral motifs, whose scattering intensity scales with the SiO_2 content. The second involves localized vibrations of the network-modifying cations along with non-bridging oxygens, whose frequency decreases and intensity increases with increasing size of alkali cations [17]. However, the frequency shift is not obvious in Fig. 1, as also stated in [18]. **To better evaluate the intensity of the peaks and their amplitude,** Cole-Cole plots **are introduced** in Subsection 3.1.

The second resonance or ionic resonance, occurs between 13 and 14 THz, and it is due to the Si-O-Si bending vibration. It arises from oscillations in the Si-O-Si bond angle within the three-dimensional silica network. As the bond bends, the oxygen atom vibrates out of the plane defined by the O-Si-O linkage. It exhibits strong infrared (IR)

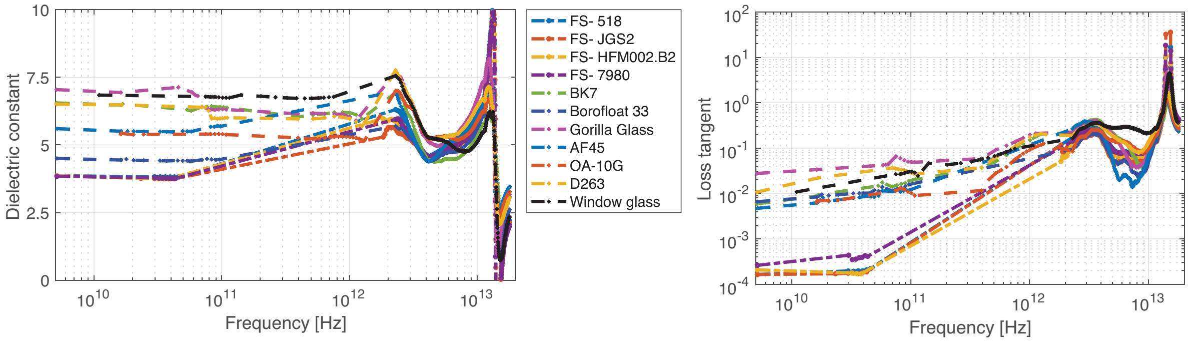

(a) (b)

Figure 1. (a) Dielectric constant and (b) loss tangent of the different silicates as a function of frequency.

intensity due to the large dipole moment changes from the oxygen atom motion. The vibration is delocalized since all Si-O-Si links vibrate in phase across the disordered network. Broadening and intensity variations provide insight into bond angle distributions and disorder. In the materials selected, the intensity of the resonance is more prominent for purer materials, i.e. the fused silicas. It is worth highlighting that the dielectric constants of the various silicate materials converge to very similar values in the terahertz frequency range, despite exhibiting some differences at lower frequencies. **For this reason, it is important to consider the effect of boson peak to characterize the dielectric properties in the mm-wave and sub-THz spectrum.**

To obtain the general dielectric response for the different amorphous silicate families, the dielectric properties of several commercial glasses and fused silicas have been averaged, respectively. The log-log complex permittivity is shown in Fig. 2. The linear frequency of the ionic resonance peak corresponds to at 13.8 THz and the boson peak at 2.5 THz. The ionic resonance is due to the Si-O-Si bending vibration. **In an attempt to evaluate whether**

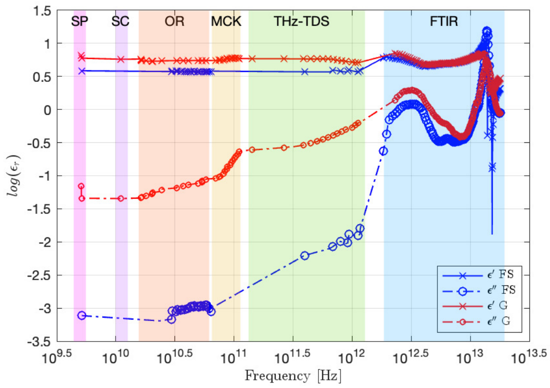

Figure 2. Log-log plot of the complex permittivity as a function of frequency. FS corresponds to the average contribution of the fused silicas, and G to the average of the commercial glasses. **The shading areas represent the measurement technique employed. SP corresponds to split-post; SC, to split-cavity and OR, to open resonator.**

the boson peak and ionic resonance observed at terahertz frequencies adhere to Jonscher's universal model, the slopes of both their rising and falling flanks were analyzed. However, the calculated slopes exceeded a value of 1**, indicating that these THz peaks deviate from the model's predictions. It is important to note that Jonscher's model was originally developed to describe relaxation phenomena, not resonant behavior. In [4], Jonscher indicated that the high-frequency limit of the applicability of the universal model would be in the short microwave or infrared region. The results plotted in Fig. 2 show that that the limit is around** 40 **GHz.**

To model the losses in the THz range, the product of the absorption coefficient α and index of refraction n is usually plotted in literature. This model follows a power-law

$$n(f)\alpha(f) = K(hf)^{\beta} \tag{3}$$

where h is the Plank constant and K is a material-dependent absorption parameter. In [19], Strom et al. report a $\beta \leq 2$ for amorphous materials. For fused silica, they obtain a $\beta = 2$ and for Na_2O-$3SiO_2$, $\beta = 1.7$. Bagdade and Stolen use in [20] a simple charge-defect model to explain the increase absorption in glasses with the addition of modifiers. The absorption model is proportional to the square of frequency. In [2, 21], a $\beta = 2$ is found for quartz and fused silica, and $\beta = 2.6$ for BK7 glass. These values were obtained from 0.1 to 2 THz. In [22], a $\beta \sim 2$ is reported for borosilicate glasses, $1.61 \leq \beta \leq 1.95$ for tellurite glasses and $0.48 \leq \beta \leq 1.87$ for chalcogenide glasses.

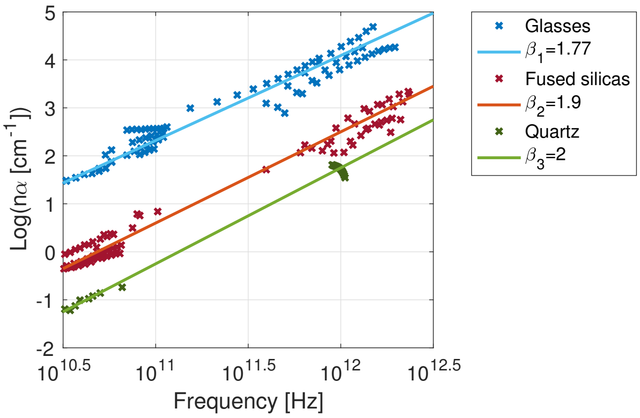

Figure 3. Measured product of absorption coefficient α and index of refraction n as a function of the frequency. Glasses and fused silicas correspond to the average of different commercial samples. The parameters β_j represent the slope of the fitted curves.

The frequency dependence of the product of the absorption coefficient α and index of refraction n has been depicted in Fig. 3, in log-log scale to facilitate the comparison with the power-law relation. Even though we have decided to include the frequency points below the THz regime, the slopes obtained align to those in [19]. The monotonically increasing loss between 40 GHz and 1 THz can be attributed to disorder-induced coupling of the electromagnetic waves to far-IR vibrational modes [19]. It is clear from Fig. 1 that the additional loss above 1 THz requires further assessment. **The key point to extract from Fig. 3 is that the THz absorption can be modelled with a power-law, on which the boson peak creates similar increasing slopes in the three different silicate groups (glasses, fused silicas and quartz), with the offset on the y-axis being the main distinction. This offset difference is related to how well-ordered the internal structure of the silicates is arranged. The higher absorption and index of refraction product values in the THz spectrum increases the product values at the mm-wave frequencies.**

3.1. Cole-Cole diagram

Several models, such as the Cole-Cole [23], Cole-Davison [24] and Havriliak-Negami [25], have been proposed in literature to model the relaxation behavior of the complex permittivity. Modifications can be made to the model to adjust to a resonant response. Born and Wolf suggested a model to represent the resonance behavior of the complex permittivity [26]

$$\epsilon^* = \epsilon_\infty + \frac{(\epsilon_0 - \epsilon_\infty)}{1 - (f/f_r)^2 + j\gamma f/f_r^2}, \tag{4}$$

with the empirical constant γ being the damping factor of the resonance and representing the half-bandwidth of peak in the imaginary part of the permittivity. ϵ_0 and ϵ_∞ are the permittivities at zero and infinite frequencies, and f_r is the resonance frequency. A modified model was proposed by Choi et al. in [27] to correct some deviation from the experimental values

$$\epsilon^* = \epsilon_\infty + \frac{(\epsilon_0 - \epsilon_\infty)}{[1 - (f/f_r)^2 + j\gamma f/f_r^2]^\kappa}. \tag{5}$$

The empirical constant κ is introduced to include the asymmetry, and to show the deviation from the regular circle, and $0 < \kappa \leq 1$. A higher γ represents a higher damping factor, which leads to a circle with smaller radius in the Cole-Cole plot and a lower loss peak intensity, with broader half-width maximum, in the imaginary spectrum.

The Argand representation (Cole-Cole diagram) of the real and imaginary parts of the permittivity is useful to provide information about the nature of the dielectric relaxations, which are common at the lower parts of the spectrum. These overdamped relaxations result in semicircular traces in the complex plane. On the other hand, from THz frequencies, resonances appear in the dielectric constant, corresponding to an oscillatory time domain response. These resonances trace like a circle in the Argand plot. Cole-Cole plots are frequently employed at very low frequencies. However, in this paper, we introduce the complex plane representation of the dielectric properties to provide more comprehension about the Boson peak and ionic resonance dynamics.

In Fig. 4(a), the imaginary part of the permittivity is plotted as a function of the real part in the whole measured spectrum. We have chosen the glass AF45 as an example to explain the diagram, as its shape differs from the typical low-frequency ones. Fig. 4(b) shows the frequency response of the corresponding imaginary part of the permittivity. The first part of the spectrum, marked in solid red line, covers from 5 GHz **up to** 1.5 THz. In the Argand plot, that part corresponds to the parallel features to the real axis, with an imaginary part close to zero. As the frequency increases,

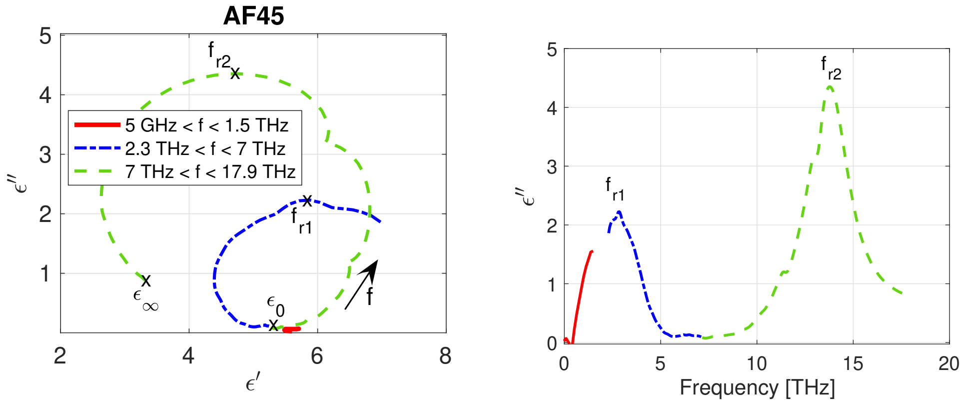

Figure 4. (a) Argand plot and (b) imaginary part of the permittivity vs. frequency of AF45 glass.

we reach the boson peak, marked in dash-dotted blue line in Fig. 4(b). This part is also marked in the complex plot, and yields a semicircular/oval shape. Frequency increases counterclockwise in these plots. Marked in Fig. 4 in green dashed line is the response from 7 THz and higher, where the loss peak associated with the ionic resonance appears. The resonance has a circular shape in the complex plane. The apex of the semicircles/circles in the Argand plots correspond to the relaxation/resonance frequencies in the frequency response.

Now that the example has been analyzed, we can compare the dielectric responses of different silicate families. Fig. 5 (a) presents the Cole-Cole plot associated with the linear dielectric properties extracted from Fig. 2. The larger circles in fused silicas and glasses correspond to the ionic resonance. It is worth emphasizing that even though fused silicas are purer than commercial glasses, in the Si-O-Si bending vibration, their losses are higher. The smaller ovals coincide with the boson peak. The depolymerization of the silica network in commercial glasses causes higher losses in the boson peak area compared to fused silicas. As mentioned earlier, the pinnacle of the circles correspond to the resonance peaks, which are 2.5 and 13.8 THz, for both glasses and fused silicas. Apart from the semicircles, the parallel features to the real axis correspond to the lower frequency range (from 5 – 40 GHz), where the dielectric response from Fig. 1 is frequency independent. **The complex plot can provide a clearer representation of the intensity and width of the peaks from the permittivity response, as the parameter γ inversely relates to the full width at half maximum. The Cole-Cole plots allow easier fitting of the dielectric response of a material. Fig. 5 (b) shows the comparison between the measured averaged responses and the calculated values obtained from Choi's model. The γ values at the boson peak are larger than those at the ionic resonance, yielding**

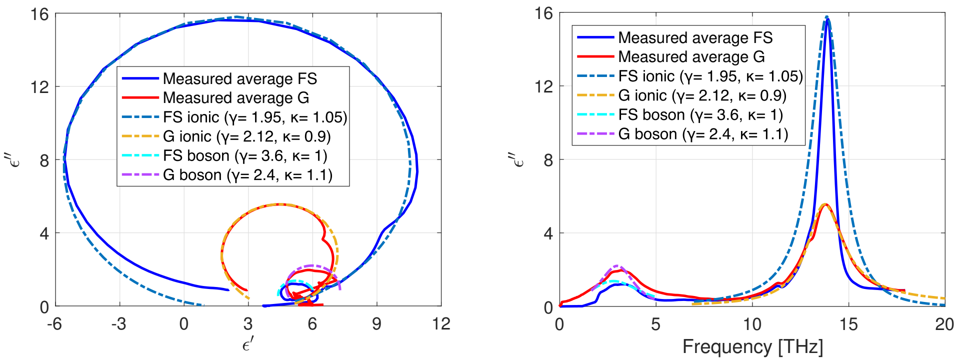

(a) (b)

Figure 5. **(a) Complex plot of the dielectric properties of fused silicas and glasses, comparing with the calculated values from Choi's model. FS corresponds to the average contribution of the fused silicas, and G to the average of the commercial glasses. (b) Corresponding imaginary part of the permittivity as a function of the frequency, comparing with the calculated values.**

broader peaks with lower intensity. For the ionic resonance of fused silicas, a κ value greater than 1 is chosen, deviating from the initially established range of $0 < \kappa \leq 1$, to better adjust the top part of the circle and provide a better overall fit. The asymmetry of ϵ_∞ is the reason the peak width is not better fitted in Fig. 5 (b). It is possible to see that **the shape of the circles is not perfect and they seem to be composed of several semicircles**, which indicate a distribution of relaxation times [28]. **Introducing network modifiers or formers into the silica network creates new local environments with different bond lengths, angles and polarizability. These configurations introduce new vibrational modes in the glass network, which can respond to a THz electric field creating multiple relaxation processes. Both the boson peak and ionic resonance are the dominant peaks at the resonance frequencies, but they are escorted by smaller peaks, which will broaden the width of the dominant peaks. These smaller peaks are easier to identify in the complex plot.**

To further evaluate the behavior of the boson peak and the ionic resonance, we have included the Argand plot of several alkaline earth aluminosilicates. Fig. 6(a) shows the complex plot for alkaline earth aluminosilicates and

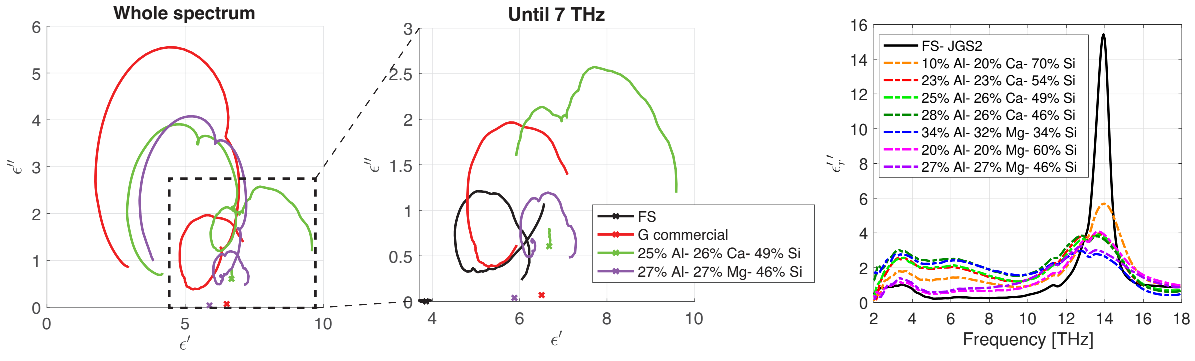

(a) (b)

Figure 6. (a) Complex plot of the dielectric properties of alkaline earth aluminosilicates, and zoomed version of the spectrum **up to** 7 THz on the right. (b) Frequency response of the imaginary part of the permittivity comparing JGS2 fused silica and the alkaline earth aluminosilicates.

Fig. 6(b), the frequency response of the imaginary part of the permittivity. Fused silica has not been plotted in the complex plot of the full spectrum due the large size of the circle, but it is included in the complex spectrum **up to** 7 THz (to see the whole spectrum of FS, please refer to Fig. 5). From all the commercial glasses averaged, AF45 is the one with the lowest silica content, 51%. The rest of the glasses are above 60%. The alkaline earth compositions shown have a maximum of 49% SiO_2 (the legend in the figure has been shortened to only the element, Si, but refers to the oxides in all the cases). For this reason, the intensity of their ionic resonance is even lower than in commercial glasses. It can be seen that there is another peak (at 12.77 THz) before the ionic resonance, at 13.7 THz. The extra peak could be attributed to lattice vibrations involving modifier cations [29]. The lighter mass of magnesium shifts its vibration to higher frequencies, causing it to overlap with the low-frequency shoulder of the broader network-bending resonance [30]. In the zoomed part, in this case, the boson peak intensity is increasing with the cation size. It is possible to see that there is also another peak (at 6.3 THz) after the boson peak (at 3.34 THz), which could be also attributed to some vibrational modes of the cation modifiers. For calcium-containing glasses, the cation vibration mode is particularly prominent. As discussed earlier, [17] claimed that the intensity of the boson peak increases with increasing size of alkali cations. Besides, the polarizability of the calcium ion is larger than the magnesium one, as shown in [31], which could explain the higher losses. However, further modeling and theoretical work is required to advance fundamental understanding of the terahertz polarization mechanisms these peaks signify. Nonetheless, the comprehensive spectroscopy and data compiled here establishes an empirical foundation for future studies to probe the physics underpinning the dielectric response as the electromagnetic waves impinging on the silicates increase from microwave to optical frequencies.

4. Conclusions

In conclusion, this work has presented unprecedented broadband dielectric characterization of various silicate materials spanning gigahertz to terahertz frequencies. Also several representations of the dielectric properties have been included to allow easier comparison with literature. The metrology results revealed a **frequency independent** dielectric response up to around 40 GHz for all silicates. Two distinct resonances emerge at higher frequencies – the boson peak around 2 THz and the Si-O-Si bending vibration around 13 THz. Constructing Cole-Cole plots from the measured data provided insight into the boson peak relaxation dynamics. Its behaviour in the complex plane resembles more distributed relaxations than a resonance.

Remarkably, while the silicates span amorphous structures with different purity and diverse compositions, their dielectric properties follow a common underlying trend. The flat, slowly varying response up to mm-waves likely stems from polarization mechanisms involving charge defects and their local environments. At terahertz frequencies, the vibrational modes tied to the cation motions and silica network, respectively, manifest.

By stitching together a broadband dielectric spectrum, this work clarifies both the commonalities and composition-specific differences in the GHz-THz behavior of the silicate family. The measurement results provide new understanding of silicate polarization while enabling more accurate modeling, simulation, and engineering of silica-based devices across microwave, terahertz, and optical frequencies.

Acknowledgements

This work was supported in part by the National Science Foundation as part of the Center for Dielectrics and Piezoelectrics under Grant Nos. IIP-1841453 and IIP-1841466, and by a research grant (41389) from VILLUM FONDEN.

The authors would like to thank Venkatraman Gopalan, Xiaojiang Li and Stephanie Law for their help with the THz-TDS and FTIR instrumentation. The authors would also like to thank Lisa Lamberson for supplying the alkaline earth silicate samples.

References

[1] G. P. Williams, Filling the thz gap—high power sources and applications, Reports on Progress in Physics 69 (2) (2005) 301.
[2] M. Naftaly, R. E. Miles, Terahertz time-domain spectroscopy for material characterization, Proceedings of the IEEE 95 (8) (2007) 1658–1665.
[3] K. Kanehara, S. Urata, S. Yasuhara, T. Tsurumi, T. Hoshina, Dielectric property and polarization mechanism of sodium silicate glass in ghz–thz range, Japanese Journal of Applied Physics 61 (SN) (2022) SN1001.
[4] A. K. Jonscher, Dielectric relaxation in solids, Journal of Physics D: Applied Physics 32 (14) (1999) R57.
[5] A. K. Jonscher, Low-loss dielectrics, Journal of materials science 34 (1999) 3071–3082.
[6] A. K. Jonscher, Energy criterion in the interpretation of dielectric relaxation, Applied Physics A 56 (1993) 405–408.
[7] A. K. Jonscher, The universal dielectric response and its physical significance, IEEE Transactions on Electrical Insulation 27 (3) (1992) 407–423.

[8] A. K. Jonscher, Low-frequency dispersion in volume and interfacial situations, Journal of Materials Science 26 (1991) 1618–1626.
[9] C. McIntosh, J. Toulouse, P. Tick, The boson peak in alkali silicate glasses, Journal of non-crystalline solids 222 (1997) 335–341.
[10] F. L. Galeener, Band limits and the vibrational spectra of tetrahedral glasses, Physical Review B 19 (8) (1979) 4292.
[11] Y. Onodera, S. Kohara, P. S. Salmon, A. Hirata, N. Nishiyama, S. Kitani, A. Zeidler, M. Shiga, A. Masuno, H. Inoue, et al., Structure and properties of densified silica glass: characterizing the order within disorder, NPG Asia Materials 12 (1) (2020) 85.
[12] M. T. Lanagan, L. Cai, L. A. Lamberson, J. Wu, E. Streltsova, N. J. Smith, Dielectric polarizability of alkali and alkaline-earth modified silicate glasses at microwave frequency, Applied Physics Letters 116 (22) (2020) 222902.
[13] R. Rodriguez-Cano, S. E. Perini, B. M. Foley, M. Lanagan, Broadband characterization of silicate materials for potential 5g/6g applications, IEEE Transactions on Instrumentation and Measurement 72 (2023) 1–8. doi:10.1109/TIM.2023.3256463.
[14] L. Duvillaret, F. Garet, J.-L. Coutaz, Influence of noise on the characterization of materials by terahertz time-domain spectroscopy, JOSA B 17 (3) (2000) 452–461.
[15] P. Nilsson, L. Munkby, Investigation of errors in the kramers-kronig analysis of reflectance data, Physik der kondensierten Materie 10 (1969) 290–298.
[16] R. Rodriguez-Cano, M. Lanagan, S. Perini, X. Li, V. Gopalan, Broadband dielectric characterization of glasses and other silicates up to the thz frequencies, in: 2023 IEEE International Symposium on Antennas and Propagation and USNC-URSI Radio Science Meeting (USNC-URSI), 2023, pp. 287–288. doi:10.1109/USNC-URSI52151.2023.10237692.
[17] N. F. Richet, Boson peak of alkali and alkaline earth silicate glasses: Influence of the nature and size of the network-modifying cation, The Journal of Chemical Physics 136 (3) (2012).
[18] Y. Duan, Y. Fujii, S. Kitani, H. Hijiya, A. Koreeda, J.-H. Ko, Y. Yamamoto, T. Mori, Terahertz dynamics of sodium silicate glass investigated by terahertz time-domain spectroscopy, in: 2021 46th International Conference on Infrared, Millimeter and Terahertz Waves (IRMMW-THz), IEEE, 2021, pp. 1–2.
[19] U. Strom, J. Hendrickson, R. Wagner, P. Taylor, Disorder-induced far infrared absorption in amorphous materials, Solid State Communications 15 (11-12) (1974) 1871–1875.
[20] W. Bagdade, R. Stolen, Far infrared absorption in fused quartz and soft glass, Journal of Physics and Chemistry of Solids 29 (11) (1968) 2001–2008.
[21] M. Naftaly, R. Miles, Terahertz time-domain spectroscopy: A new tool for the study of glasses in the far infrared, Journal of non-crystalline solids 351 (40-42) (2005) 3341–3346.
[22] N. J. Tostanoski, S. Sundaram, Universal power-law of terahertz optical properties of borosilicate, tellurite, and chalcogenide glass families, Scientific Reports 13 (1) (2023) 2260.
[23] K. S. Cole, R. H. Cole, Dispersion and absorption in dielectrics i. alternating current characteristics, The Journal of chemical physics 9 (4) (1941) 341–351.
[24] D. Davidson, R. Cole, Dielectric relaxation in glycerine, J. Chem. Phys 18 (1951) 1417.
[25] S. Havriliak, S. Negami, A complex plane representation of dielectric and mechanical relaxation processes in some polymers, Polymer 8 (1967) 161–210.
[26] M. Born, E. Wolf, Principles of Optics, Pergamon Press, Oxford, 1959.
[27] H. D. Choi, K. Y. Cho, S. Han, H. G. Yoon, T. J. Moon, Frequency dispersion characteristics of the complex permittivity of the epoxy-carbon black composites, Journal of applied polymer science 67 (2) (1998) 363–369.
[28] P. Mantas, Dielectric response of materials: extension to the debye model, Journal of the European Ceramic Society 19 (12) (1999) 2079–2086.
[29] A. R. Allu, A. Gaddam, S. Ganisetti, S. Balaji, R. Siegel, G. C. Mather, M. Fabian, M. J. Pascual, N. Ditaranto, W. Milius, et al., Structure and crystallization of alkaline-earth aluminosilicate glasses: prevention of the alumina-avoidance principle, The Journal of Physical Chemistry B 122 (17) (2018) 4737–4747.
[30] C. I. Merzbacher, W. B. White, The structure of alkaline earth aluminosilicate glasses as determined by vibrational spectroscopy, Journal of Non-Crystalline Solids 130 (1) (1991) 18–34.
[31] R. D. Shannon, Dielectric polarizabilities of ions in oxides and fluorides, Journal of Applied physics 73 (1) (1993) 348–366.